# A Novel Secondary Frequency Regulation with Optimal Priority Selection of AGC Contributions

Sufan Jiang, Linquan Bai
*University of North Carolina at Charlotte*
Charlotte, North Carolina, USA
{sjiang10;lbai4}@uncc.edu

Hong Wang, Yonghao Gui, Yaosuo Xue
*Oak Ridge National Laboratory*
Oak Ridge, Tennessee, USA
{wangh6;guiy;xuey}@ornl.gov

***Abstract*—Automatic generation control (AGC) is used to maintain acceptable frequencies during operation owing to fluctuations in load and variable resources. In conventional industry applications, the AGC signal is allocated to each generator according to the predispatched frequency regulation capacity or the order of economic efficiency. However, with the increasing integration of inverter-based resources (IBRs), the retirement of conventional synchronous generators (SGs) has posed new challenges to frequency control schemes because fewer of them are optional for AGC regulation. In this paper, we propose a novel model predictive control (MPC)-based frequency regulation model to reduce control cost and ensure stability, by considering different critical dynamic factors when optimally selecting the AGC units. The proposed control model – developed in a general form – comprehensively embeds characteristics such as generator ramping rates, reserve capacity, and operation cost. The model predictive control–based two-timescale AGC scheme enhances the capability of immunizing the power disturbance from types of resources by coordinating the control signals between faster IBRs and slower SGs. The case study's proposed model is verified to be effective in synergistically enforcing different dynamic properties of AGC units into the frequency regulation scheme.**

***Index Terms*—Automatic generation control (AGC), inverter-based resource (IBR), frequency regulation, units priority selection, model predictive control (MPC)**

## I. Introduction

The increasing penetration of renewable energy sources (RESs) gradually reduces rotational inertia and increases and exacerbates the consequences of power disturbances, posing further challenges to frequency stability issues. Power systems generally rely on three different timescales of responses: primary, secondary, and tertiary frequency regulations.

Secondary frequency regulation, also called automatic generation control (AGC), is used to maintain acceptable frequencies during operation owing to fluctuations in load and variable resources. In PJM, the AGC solution is proposed to separate a regulation signal into a slow-responding signal RegA and a fast-responding signal RegD, which are generated from low and high-pass filtering, respectively, after a proportional-integral-derivative controller [1], [2]. The RegD signal containing high-frequency components can take advantage of the fast response of fast units. In New York Independent System Operator (NYISO), the AGC and real-time dispatch programs assign base points to resources based on their response rates and energy levels, adjusting these points during reserve pick-ups or events. The NYISO's Performance Tracking System monitors and influences resource performance, determining payments, penalties, and movement instructions for regulation service providers [3].

However, a concerted effort is underway to phase out fossil fuel–based generation in favor of inverter-based resources (IBRs) [4]. Because of the increasing penetration of RES, the low inertia of power systems has brought significant challenges to frequency regulation, especially under extreme circumstances with low probability [5]. The retirement of conventional coal-fired plants further exacerbates the frequency stability issues, owing to restrictions of assigning them as AGC units and the lack of AGC reserve. As a result, developing a series of principles for selecting AGC units within the limited given set of generators is necessary and can be accomplished by comprehensively embedding characteristics such as generator ramping rates, reserve capacity, and operation cost.

In recent years, researchers have made remarkable studies on AGC schemes in all kinds of operation environments. Considering the flexibility and scalability of converter-based devices, the participation of IBRs, microgrids, distributed generators (DGs), and high-voltage direct currents (HVDCs) are studied within AGC schemes [6]. Different AGC market environments are discussed in [7], where the study is extended to frame and implement optimal proportional-integral (PI) regulators for the first time for the AGC of a conventional two-area, non-reheat thermal power system with governor deadband nonlinearity. To enhance the control performance of the AGC schemes, advanced algorithm and modeling methods are developed in [8] and [9], such as metaheuristic and AI-enhanced approaches. Considering the AGC schemes from an optimization perspective, the studies in [10] connect the AGC and the economic dispatch to ensure optimality of the operational schedule when integrating frequency dynamics. In [10], a bi-objective pareto AGC dispatch model is proposed, and the online performance and optimization speed are demonstrated to be superior. A comprehensive AGC model is proposed in [11], considering the coordination between conventional generators and energy storage, the ramping needs upon detecting a potentially destabilizing event are modeled. Based on this introduction, this paper aims to solve the following two aspects of research gaps:

- Current approaches focus on using the reserve capacity to select the most appropriate generation resources to ac-

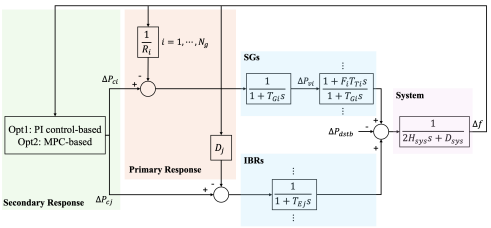


Fig. 1. Block diagram of a single-area AGC system

complish the required frequency regulation. Exploring a more comprehensive selection mechanism that considers other factors, such as cost, is needed.

- Network constraints are neglected by most previous studies, and power flow congestion has a significant effect on the effectiveness of frequency regulation. Therefore, deliverability of the frequency reserve should be highly concentrated by the AGC model.

As a result, in this paper, the authors propose a novel frequency regulation model to provide innovative guidance for how to select AGC units when considering both steady-state and dynamic factors. The proposed control model – developed in a general form – comprehensively embeds characteristics such as generator ramping rates, reserve capacity, and operation cost. The model evaluates the control performance and control cost by assigning appropriate coefficient matrices in the objective function. The model predictive control (MPC)–based two-timescale AGC scheme enhances the capability of immunizing the uncertainty of renewable energy by coordinating the control signals between faster inverter-based resources (IBRs) and slower conventional synchronous generators (SGs). The case study's proposed model is verified to be effective in synergistically enforcing different dynamic properties of AGC units into the frequency regulation scheme.

## II. State-Space Equation of System Frequency Response Model

This section describes the state-space model and its discretization of a typical system frequency response model, wherein different timescales of regulation resources – SGs and IBRs – are integrated into the AGC model.

### A. State-Space Equation

In this paper, it is assumed that the AGC scheme is implemented into a single area: the area control error consists of only the local frequency deviation, without the need for considering other factors, such as tie-line bias. The block diagram is depicted in Fig. 1. Two types of frequency regulation resources are in these control blocks: SGs with slower response rates and IBRs (such as DG and energy storage system (ESS)) with faster response rates. The SG frequency response model is described by a classical two-order governor-turbine model, and the IBR model is presented by a one-order inertial block. In the IBR's time constant, $T_{EJ}$ is in milliseconds, which is two to three orders of magnitude smaller than that in SG, which is the reason for the IBRs' faster response capability. The AGC model also includes the local primary frequency response (PFR) control loop and power ramping limiter of each unit.

The state-space model of the AGC system in Fig. 1 can be formulated as follows:

$$\dot{x}(t) = \bar{A}x(t) + \bar{B}_u u(t) + \bar{B}_w w(t), \tag{1}$$

where

$$x(t) = \begin{bmatrix} \Delta f(t) & \Delta P_G(t)^T & \Delta P_E(t)^T \end{bmatrix}^T, \tag{2}$$

$$\Delta P_G(t) = [\cdots \ \Delta P_{vi}(t) \ \Delta P_{mi}(t) \ \cdots]^T, \tag{3}$$

$$\Delta P_E(t) = [\cdots \ \Delta P_{mj}(t) \ \cdots]^T, \tag{4}$$

$$u(t) = \begin{bmatrix} \Delta P_{cG}(t)^T & \Delta P_{cE}(t)^T \end{bmatrix}^T. \tag{5}$$

The system states $x(t)$ include the frequency deviation $\Delta f$, SG states $\Delta P_G$ (valve opening, mechanical power change), and IBR states $\Delta P_E$ (electric power change). The AGC signals $u(t)$ decided in the control center contain the control signals of SG ($\Delta P_{cG}$) and IBR ($\Delta P_{cE}$). The coefficient matrices extracted from the control block in Fig. 1 are $\bar{A}$, $\bar{B}_u$, and $\bar{B}_w$. The size of the state matrix $\bar{A}$ is $(1+2N_g+N_e)\times(1+2N_g+N_e)$; it is decomposed into nine submatrices corresponding to $\Delta f$, $\Delta P_G$, and $\Delta P_E$. In addition, $\bar{B}_u$ and $\bar{B}_w$ are input matrices for AGC signals $u(t)$ and power disturbance $w(t)$, respectively, where $w(t)$ is explained by $\Delta P_e$ in the control block. Also, $\Delta P_{cG}(t)$ is the vector of $\Delta P_{ci}(t)$, which is the control reference to SG $i$; $\Delta P_{cE}(t)$ is the vector of all $\Delta P_{cj}(t)$, which is the control reference to IBR $j$.

### B. Discretization of Frequency Response Model

Based on the zero-order hold method, the solution of the control system can be derived from (1) as

$$x(t) = e^{\bar{A}(t-t_0)}x(t_0) + \int_{t_0}^{t} e^{\bar{A}(t-\varphi)}\bar{B}u(\varphi)\,d\varphi. \tag{6}$$

For the discrete sampled-data system, we substitute $t$ and $t_0$ with $nT$ and $nT+T$, where $T$ is the sampling period, and then we can get

$$x(nT+T) = e^{\bar{A}T}x(nT) + \int_{nT}^{nT+T} e^{\bar{A}(nT+T-\varphi)}\bar{B}u_n\,d\varphi. \tag{7}$$

Letting $\theta = nT + T - \varphi$, we can get the discrete form

$$x_{n+1} = e^{\bar{A}T}x_n + \int_{\theta}^{T} e^{\bar{A}\theta}d\theta\bar{B}u_n. \tag{8}$$

As a result, we can obtain the matrices from the following:

$$A = e^{\bar{A}T}, \tag{9}$$

$$B_u = \int_0^T e^{\bar{A}\theta}d\theta\,\bar{B}_u = \left(e^{\bar{A}T} - I\right)\bar{A}^{-1}\bar{B}_u, \tag{10}$$

$$B_w = \int_0^T e^{\bar{A}\theta}d\theta\,\bar{B}_w = \left(e^{\bar{A}T} - I\right)\bar{A}^{-1}\bar{B}_w. \tag{11}$$

Finally, the compact form can be derived from

$$x_{n+1} = Ax_n + B_u u_n + B_w w_n. \tag{12}$$

The methods of integrating the frequency response model into the optimal AGC will be introduced in Section III.

## III. MPC-Based Optimal Control Model

To develop the novel AGC model motivated by the research gaps described in Section I, we designed an optimal control model based on MPC and integrated various dynamic characteristics into the objective function. The detailed model is described in this section.

### A. Optimal MPC Control Model

Based on the discrete state-space model, the MPC-based AGC model is formulated as the following optimization program:

$$\min \left[ J = \gamma \sum_{n=1}^{N_p} x_n^T \mathbb{C}^T \mathbb{C} x_n + \sum_{n=0}^{N_c-1} u_n^T \mathbb{R} u_n \right], \tag{13}$$

$$s.t. \quad x_{n+1} = Ax_n + B_u u_n + B_w w_n, \quad n = 0, 1, \ldots, N_p - 1, \tag{14}$$

$$-\Delta f_{lim} \le (\Delta f)_n \le \Delta f_{lim}, \tag{15}$$

$$I_i \cdot \underline{\Delta P_{ci}} \le (\Delta P_{ci})_n \le I_i \cdot \overline{\Delta P_{ci}}, \quad n = 0, \ldots, N_c - 1, \tag{16}$$

$$\underline{\Delta P_{cj}} \le (\Delta P_{cj})_n \le \overline{\Delta P_{cj}}, \quad n = 0, \ldots, N_c - 1, \tag{17}$$

$$I_i \cdot Rd_i \le (\Delta P_{mi})_n - (\Delta P_{mi})_{n-1} \le I_i \cdot Ru_i, \quad n = 1, \ldots, N_p, \tag{18}$$

$$Rd_j \le (\Delta P_{mj})_n - (\Delta P_{mj})_{n-1} \le Ru_j, n = 1, \ldots, N_p, \tag{19}$$

$$\sum\nolimits_{i=1}^{N_g} I_i \le N_{AGC}, \tag{20}$$

$$\sum_{i=1}^{N_g} \Delta P_{ci} \cdot GSF_{i-l} + \sum_{j=1}^{N_e} \Delta P_{cj} \cdot GSF_{j-l} \le \overline{\Delta F_l} \quad l = 1, \ldots, N_l, \tag{21}$$

where $x(n)$ and $u(n)$ in the objective function are the system state and the control input in $n$-th time step, respectively; and $N_p$ and $N_c$ are the numbers of prediction steps and control steps in MPC, respectively. The objective function consists of two parts: the control performance and the control cost; the performance cost matrix $\mathbb{C} = \begin{bmatrix} 1 & \mathbf{0}_{1\times(2N_g+N_e)} \end{bmatrix}$ considers only the frequency performance of all system states. In addition, $\gamma$ is a weighting factor to ensure that the first and second terms are comparable. The control cost matrix $\mathbb{R}$ is a diagonal positive-definite matrix; its submatrices $\mathbb{R}_G$ and $\mathbb{R}_E$ correspond to SGs and IBRs, respectively, which are defined as follows:

$$\mathbb{R} = \begin{bmatrix} \mathbb{R}_G & \mathbf{0}_{N_g \times N_e} \\ \mathbf{0}_{N_e \times N_g} & \mathbb{R}_E \end{bmatrix}, \tag{22}$$

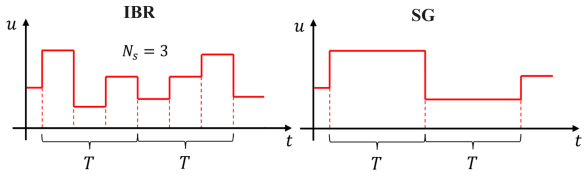


Fig. 2. AGC signals of IBRs and SGs.

$$\mathbb{R}_G = diag\left\{ \cdots \frac{\sigma_i}{\min(\Delta P_{ci}, -\Delta \underline{P}_{ci})} + C_i^{AGC} \cdots \right\}, \tag{23}$$

$$\mathbb{R}_E = diag\left\{ \cdots \frac{\sigma_j}{\min(\Delta P_{cj}, -\Delta \underline{P}_{cj})} + C_j^{AGC} \cdots \right\}. \tag{24}$$

The diagonal element in $\mathbb{R}_G$ and $\mathbb{R}_E$ consists of two parts: the reciprocal of the regulation capacity of each unit (denoted as $\min(\Delta P_{ci}, -\Delta \underline{P}_{ci})$) and the dispatching cost of the AGC reserve per unit $C_j^{AGC}$. Furthermore, $\sigma$ is the weighting factor for comprehensively considering these two factors. The control goal of AGC is to drive the system frequency back to the reference value, which is reflected in the control performance in (13). The coefficient matrix $\mathbb{R}$ for control variable $u_n$ can ensure that the AGC signal is allocated to each unit according to both the regulation capacity and the dispatching cost. The unit with a larger regulation capacity and lower control cost will be assigned more AGC responsibility. Constraint (14) is the discrete state space model. Other operational constraints are the frequency deviation limits (15), $\Delta f_{lim}$ is bound of the frequency deviation; The output of the generators are bounded by $\underline{\Delta P_{ci}}$ and $\overline{\Delta P_{ci}}$ in (16)–(17); The ramping rates are limited by $\overline{Rd_j}$/$Ru_j$ in (18)–(19). Note that the binary variable $I_i$ in constraint (20) is the status of whether a unit is assigned as an AGC unit; the total allowed number of participated-AGC unit is denoted by $N_{AGC}$. Constraint (21) is the proposed network constraint for the AGC model, where $GSF$ is the generation shift factor used for calculating the sensitivities of the power flow to the nodal injection power, $\overline{\Delta F_l}$ is the maximum accepted power increments on transmission line $l$, and $N_l$ is the number of transmission lines.

### B. Multi-Timescale AGC Model

Considering that the IBRs have a response much faster than that of SGs within the AGC model, control flexibility could be exploited if the control references of IBRs are updated faster than those of the conventional update period. In this paper, in each control reference update period $T$, the control signal of an IBR is evenly decomposed into $N_s$ segments, as shown in Fig. 2. As a result, the multistep signals are delivered to IBRs, and the single-step signals are sent to SGs.

According to the model introduction presented earlier in this paper, the resultant multitimescale AGC model is reformulated as follows:

$$\min \left[ J = \gamma \sum_{l=1}^{N_p \times N_s} x_l^T \mathbb{C}^T \mathbb{C} x_l + \sum_{l=0}^{N_c \times N_s - 1} u_l^T \mathbb{R} u_l \right], \tag{25}$$

TABLE I
DYNAMIC PARAMETERS OF SGS

| Droop | Governor | Turbine | Fraction |
|---|---|---|---|
| $\frac{1}{R_i}$ (p.u.) | time $T_{Gi}$ (s) | time $T_{Ti}$ (s) | $F_i$ (p.u.) |
| 15–30 | 0.5–0.6 | 7–15 | 0–0.25 |

$$s.t. \quad x_{l+1} = Ax_l + B_u u_l + B_w w_l, \\ n = 0, 1, \ldots, N_p \times N_s - 1, \tag{26}$$

$$G_x x_l \leq g_x, \quad l = 1, \ldots, N_p \times N_s, \tag{27}$$

$$G_u u_l \leq g_u, \quad l = 0, \ldots, N_c \times N_s - 1, \tag{28}$$

$$G_g \left(u_l - u_{l-1}\right) = 0, \\ l = 1, \ldots, N_s - 1, N_s + 1, \ldots, 2N_s - 1, \ldots. \tag{29}$$

The objective function (25) includes $N_p \times N_s$ predicted system states; therefore, the index of each state is switched as $l$. (27) and (28) are the compact forms of the operational constraints for SGs and IBRs, which are similar to those in (15)–(19). Note that the additional constraints (29) ensure that the $N_s$ control references for SGs should be identical in a control period, denoted as:

$$(\Delta P_{ci})_n^k - (\Delta P_{ci})_n^{k-1} = 0, \\ k = 1, 2, \ldots, N_s - 1, \quad n = 1, 2, \ldots, N_c. \tag{30}$$

In our model, the sampling and updating periods of multi-timescale AGC are kept the same as those in the conventional AGC model, remaining unchanged except for the quantity of decision variables increasing $N_s$ times. At each AGC updating period, the control center sends a set of single-step control references to SG and a multi-step ($N_s$ steps) control reference to IBR.

## IV. CASE STUDY

In this section, to validate the effectiveness of our proposed MPC-based AGC model, we use the conventional PI control-based AGC model as a reference, where the participation factors of each unit are proportional to the AGC reserve capacity. Our model, implemented on MATLAB R2024a, is tested on a smaller test system and a larger IEEE 118 system.

### A. Smaller Test System

In this subsection, our proposed model is tested on a system with three SGs and two IBRs; the specific dynamic parameters for the generator units are listed in Tables I and II. The control horizon is 160 s, the AGC period is set as 5 s, the total inertia $H_{sys}$ is 5.73 s, and the load damping $D_{sys}$ is set to 1 p.u.; the maximum tolerated frequency threshold $\Delta f_{lim}$ is 0.2 Hz. For the MPC model in the proposed model, the numbers of prediction and control steps are set as $N_p = 3$ and $N_c = 3$, respectively.

The power disturbance curves and the resultant frequency curves of two test cases are given in Fig. 3. The figure illustrates that the dynamic performance of the proposed model

TABLE II
DYNAMIC PARAMETERS OF IBRS

| Droop $D_j$ (p.u.) | Time constant $T_{Ej}$ (s) |
|---|---|
| 6–8 | 0.1–0.15 |

is much better than that of the conventional PI control-based AGC. As shown in the comparison, the frequency deviation is smoother in our model; it fluctuates near the nominal value even though the power disturbance has an obvious variation over time. The frequency deviations are subject within ±0.15 Hz. Although the PI parameters are tuned extensively in our test case, they are not dynamically adaptive to uncertainty scenarios, especially when the tuned PI parameters are kept fixed during the operation. The proposed model's control performance is drastically enhanced when integrating it into the objective function.

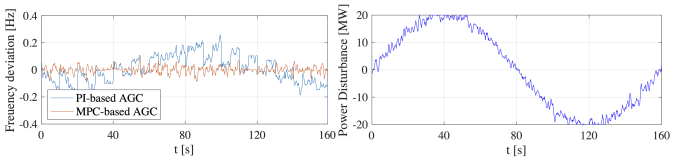


Fig. 3. Frequency evolution and power disturbance in a smaller test system.

In Fig. 4 and Fig. 5, we present the control references and the system state variables of two test models; only the curves of SG1 and IBR1 are given in the figures for the sake of clarity. The limited control capability of PI-based AGC is revealed in comparison. As shown by the results, in the PI-based AGC, the SG control references tend to follow the trends of the power disturbance variation, whereas the control references of IBRs vary less than those in the proposed MPC-based AGC. This indicates that the controllability of the IBRs did not receive full exploitation.

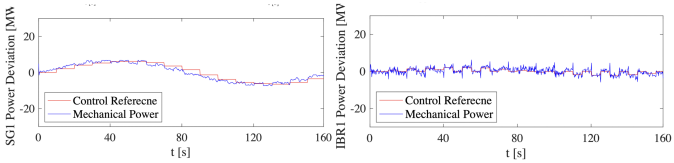


Fig. 4. Control reference and mechanical power (SG1 and IBR1) of the PI-based AGC.

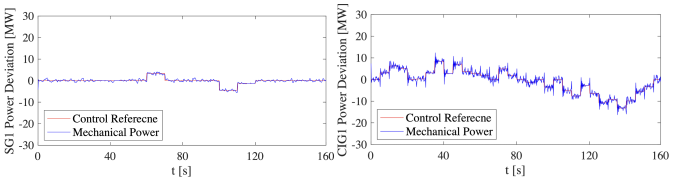


Fig. 5. Control reference and mechanical power (SG1 and IBR1) of the proposed AGC model.

In other words, in our proposed model (Fig. 5), the IBR is able to participate in more regulation works owing to

its control flexibility (especially with the multistep control reference), and the SG is thereby assigned fewer control commands by the operator. As a result, the MPC-based AGC model optimizes the control reference in a globally comprehensive consideration by enforcing control performance into the objective function.

### *B. Larger IEEE 118-Bus Test System*

The larger test system has 54 SGs and 10 IBRs, including 16 SGs and 4 IBRs equipped with AGC functions. The dynamic parameters of generator units are referred to in [11]. The control performance (frequency deviation) and the induced power disturbance after applying our proposed model on the larger test system are illustrated in Fig. 6.

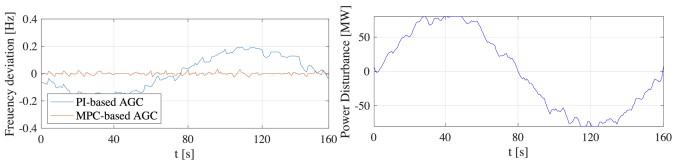


Fig. 6. Frequency evolution and power disturbance in a larger test system.

The control performance of the proposed model is better than that of the conventional PI-based AGC. The frequency deviation is captured within $\pm 0.05$ Hz and with far fewer fluctuation than that of the frequency in the PI-based AGC. For the proposed model, parts of the output curve of the SGs and IBRs are presented in Fig. 7 and Fig. 8.

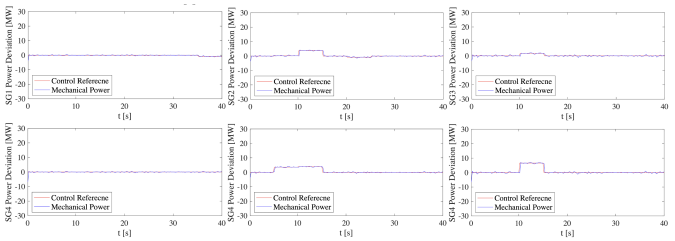


Fig. 7. Output results of SGs in an MPC-based AGC.

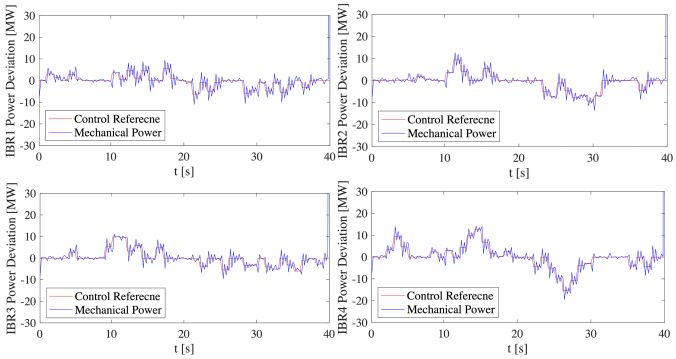


Fig. 8. Output results of IBRs in an MPC-based AGC.

In the larger test system, the frequency regulation outputs of both SG and IBR are smoother that that in the smaller system because more generation units are taking part in the regulation, and each of them becomes more efficient and capable in response. Note that SG3 and SG4 in the proposed MPC-based model did not participate in the AGC regulation owing to their lower ramping rates and higher reserve cost. This is one of the critical contribution of our model—various dynamic characteristics of the frequency response resources are integrated into it. Therefore, the advanced selection results could be made by our model, when compared with the conventional PI-based AGC.

## V. Conclusion

We propose a novel frequency regulation model that could select AGC units by considering different critical factors. Characteristics such as generator ramping rates, reserve capacity, and operation cost are integrated into the objective function. The flexibility and effectiveness of the AGC model are exploited by coordination between the SGs and IBRs and by network constraints. In our future work, we expect to study the coordination among frequency response schemes with different timescales, such as the probability distribution function frequency control.

## References


[1] PJM, "Implementation and rationale for PJM's conditional neutrality regulation signals," 2017. [Online]. Available: https://www.pjm.com/.

[2] PJM, "PJM manual 12: Balancing operations," 2023. [Online]. Available: https://learn.pjm.com/media/documents/manuals.

[3] NYISO, "NYISO manual 2: Ancillary services manual," Jul. 2019. [Online]. Available: https://www.nyiso.com/documents.

[4] K. Moustakas, M. Loizidou, M. Rehan, and A. S. Nizami, "A review of recent developments in renewable and sustainable energy systems: Key challenges and future perspective," *Renew. Sustain. Energy Rev.*, vol. 119, p. 109418, Mar. 2020.

[5] O. Stanojev, U. Markovic, P. Aristidou, G. Hug, D. Callaway and E. Vrettos, "MPC-based fast frequency control of voltage source converters in low-inertia power systems," *IEEE Trans. Power Syst.*, vol. 37, no. 4, pp. 3209-3220, Jul. 2022.

[6] Y. Gui et al., "Review of challenges and research opportunities for control of transmission grids," *IEEE Access*, vol. 12, pp. 94543-94569, 2024.

[7] R. N. Patel and V. Pant, "AGC of a multi-area multi-source hydrothermal power system interconnected via AC/DC parallel links under deregulated environment," *Int. J. Electr. Power Energy Syst.*, vol. 29, no. 10, pp. 751-759, Dec. 2007.

[8] Y. Shen, W. Wu and S. Sun, "Stochastic model predictive control based fast-slow coordination automatic generation control," *IEEE Trans. Power Syst.*, vol. 39, no. 3, pp. 5259-5271, May 2024.

[9] Q. Shen, X. Wen, S. Xia, S. Zhou, and H. Zhang, "AI-Based analysis and prediction of synergistic development trends in U.S. photovoltaic and energy storage systems," *Int. J. Innov. Res. Comput. Sci. Technol.*, vol. 12, no. 5, pp. 36–46, Sep. 2024.

[10] X. Zhang, C. Li, B. Xu, Z. Pan and T. Yu, "Dropout deep neural network assisted transfer learning for bi-objective Pareto AGC dispatch," *IEEE Trans. Power Syst.*, vol. 38, no. 2, pp. 1432-1444, Mar. 2023.

[11] Y. Xu, A. Parisio, Z. Li, Z. Dong and Z. Ding, "Optimization-based ramping reserve allocation of BESS for AGC enhancement," *IEEE Trans. Power Syst.*, vol. 39, no. 2, pp. 2491-2505, Mar. 2024.

[12] N. Li, C. Zhao and L. Chen, "Connecting automatic generation control and economic dispatch from an optimization view," *IEEE Trans. Control Netw. Syst.*, vol. 3, no. 3, pp. 254-264, Sept. 2016.

[13] I. Peña, C. B. Martinez-Anido and B. -M. Hodge, "An extended IEEE 118-bus test system with high renewable penetration," *IEEE Trans. Power Syst.*, vol. 33, no. 1, pp. 281-289, Jan. 2018.